Magnetic Nanoparticles for Ultrafast Mechanical Control of Inner Ear Hair Cells

Jae-Hyun Lee,[†] Ji-wook Kim,[†] Michael Levy,[‡] Albert Kao,[‡] Seung-hyun Noh,[†] Dolores Bozovic,[‡,§,*] and Jinwoo Cheon[†,*]

[†]Department of Chemistry, Yonsei University, Seoul 120-749, Korea, [‡]Department of Physics and Astronomy, University of California, Los Angeles, California 90095, United States, and [§]California NanoSystem Institute, University of California, Los Angeles, California 90095, United States

ABSTRACT We introduce cubic magnetic nanoparticles as an effective tool for precise and ultrafast control of mechanosensitive cells. The temporal resolution of our system is ~1000 times faster than previously used magnetic switches and is comparable to the current state-of-the-art optogenetic tools. The use of a magnetism-gated switch reported here can address the key challenges of studying mechanotransduction in biological systems. The cube-shaped magnetic nanoparticles are designed to bind to components of cellular membranes and can be controlled with an electromagnet to exert pico-Newtons of mechanical force on the cells. The cubic nanoparticles can thus be used for noncontact mechanical control of the position of the stereocilia of an inner ear hair cell, yielding displacements of tens of nanometers, with sub-millisecond temporal resolution. We also prove that such mechanical stimulus leads to the influx of ions into the hair cell. Our study demonstrates that a magnetic switch can yield ultrafast temporal resolution, and has capabilities for remote manipulation and biological specificity, and that such magnetic system can be used for the study of mechanotransduction processes of a wide range of sensory systems.

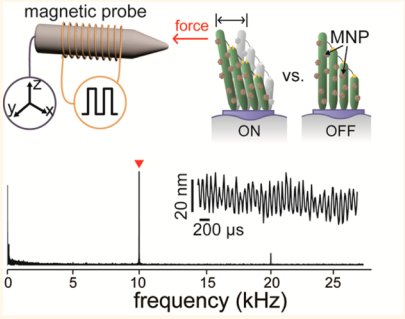

KEYWORDS: magnetic nanoparticle · magnetic stimulation · hair cell · mechanosensitive ion channel

Mechanotransduction, the conversion of a mechanical stimulus into an electrochemical signal, is important in biological systems, as it regulates the signals of touch, pain, hearing, and proprioception and the adjustment of vascular blood flow.[1,2] Mechanotransduction occurs when the application of stretch, pressure, or twist exerts a mechanical force on an ion channel, leading to a conformational change that opens the channel and allows the influx of ions.[3] Although there has been much interest in the scientific community in understanding and controlling the mechanotransduction process,[4] the development of tools with noncontact and precise spatiotemporal capabilities has posed challenges. For example, traditional tools, such as glass or piezoelectric probes, pose two intrinsic problems: they impose a mechanical load on the cells, and they can create hydrodynamic artifacts when used with fluid-immersed tissue.[5−8] While enormous progress has been made in the development of optical tools for studying light-gated ion channels of optogenetics,[9] remote and noninvasive tools with comparable spatiotemporal capabilities have not yet been realized for the study of mechanosensitive processes.

Magnetic field readily penetrates biological tissue without inducing damage in the cells; hence, it constitutes a potentially powerful tool for remote and noninvasive mechanical actuation. Magnetic fields can be applied to exert forces on magnetic nanoparticles (MNPs), which can be attached to membrane receptors or even intracellular proteins. In nature, a number of magnetosensory species, ranging from bacteria to migratory animals, use arrays of nature-built magnetic nanoparticles as a compass for navigation.[10,11] Recently, magnetic nanoparticles have been successfully adopted for biomedical studies from *in vitro* to *in vivo*.[12−20] Mannix *et al.* first demonstrated the mechanical activation of ion channels by using magnetic nanoparticle clusterization.[17] *In vivo* study of magnetothermal activation of ion channels of *Caenorhabditis elegans*,[18] magnetomechnical activation of apoptotic

* Address correspondence to bozovic@physics.ucla.edu, jcheon@yonsei.ac.kr.

Received for review April 14, 2014 and accepted June 20, 2014.

Published online July 08, 2014
10.1021/nn5020616

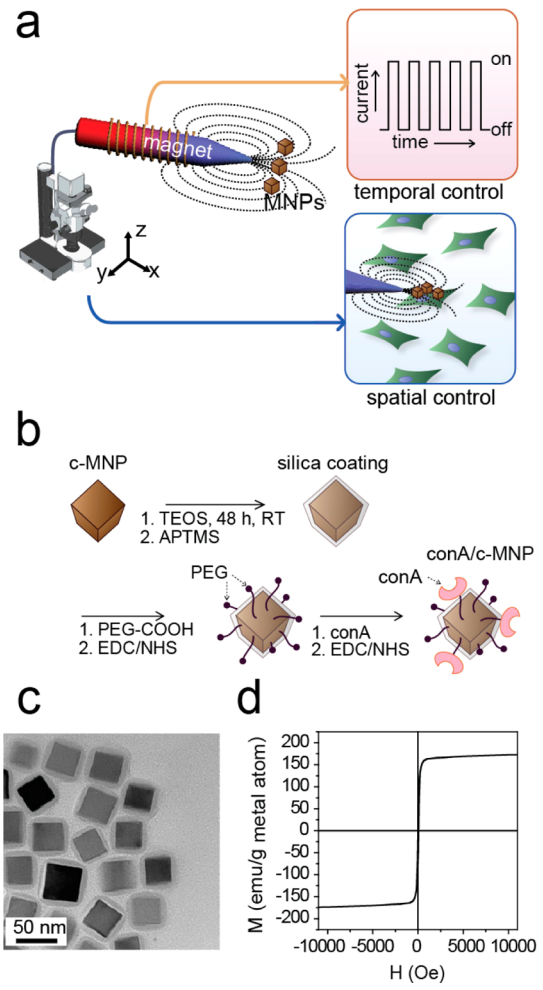

Figure 1. Cubic magnetic nanoparticle (c-MNP) mediated switch for spatiotemporal control of the mechanotransduction process. (a) Magnetic switch composed of an electromagnetic probe mounted on a micropositioner, an electric current generator, and c-MNPs. The magnetic force between the probe and the MNPs mechanically stimulates the substrate to which the particles are attached. Time-dependent magnetic field applied by the magnetic probe enables temporal and spatial control at a single-cell level. (b) Preparation scheme of c-MNP, the surface of which is sequentially modified with thin layers of silica, polyethylene glycol (PEG), and concanavalin A (conA). (c) Transmission electron microscope (TEM) image of silica-coated c-MNP with a *ca.* 45 nm edge length. (d) Magnetization curve of c-MNPs measured at room temperature.

signaling in zebrafish,[15] subcellular magnetic manipulation of Rac-GTPase signaling,[13] and magnetic control of plasma glucose levels in rodents[19] are some of the representative cases. These studies clearly demonstrate the tremendous potential of magnetic control of cellular signaling processes. However, the temporal resolution for actuating biological systems has ranged from hours[13,15] to seconds.[14,20] Hence, these techniques would not be effective as input signals for a wide range of biological systems that operate at millisecond or faster time scales. Therefore, in order to stimulate cells in a reproducible and effective manner, we needed to develop a magnetic system that can satisfy the required capability.

Our magnetism-gated switch was designed to meet the following criteria: it should exert adequate forces remotely, reversibly, in a spatially localized manner, and with a very fast response time (Figure 1a). By stimulating selected cells coated with cubic magnetic nanoparticles (c-MNPs), one can modulate the gating of mechanosensitive ion channels at a single-cell level. We demonstrated the technique at time scales that vary from slow (a few seconds) to fast (100 μs) and tested our method on inner ear hair cells. We chose hair cells as a model system since they transduce mechanical stimuli to electromechanical signal through the gating of mechanotranduction channels on the cell membrane.[21,22] Hair cells are of particular interest, since they possess one of the fastest response frequencies of any known mechanosensitive biological system. Hence, our study has a potential to impact a wide range of biological studies of mechanosensation including magnetogenetics[13] by providing the capability of fast temporal control that is now comparable to that of optogenetics.[9]

RESULTS AND DISCUSSION

Fast and Reversible Magnetic Switch: Magnetic Nanoparticles and Their Manipulation. Hair cells of the inner ear mediate the transduction of auditory and vestibular signals. The mechanotransduction channel, found in the hair bundle structure that protrudes from the hair cell soma, responds to an incoming vibration by converting the mechanical tension induced in deflected bundles into ionic currents.[21,22] We tested our magnetic switch as a new tool for mechanically stimulating hair bundles of the inner ear. For this purpose, we designed a cube-shaped MNP (c-MNP, $Zn_{0.4}Fe_{2.6}O_4$), which possesses a high magnetization value and exhibits colloidal stability (Figure 1b–d, Supporting Figure 3). The nanoparticle's shape, Zn-doped material, and size (<50 nm diameter) yielded a high saturation magnetization value (M_s), measured to be 162 emu/$g_{metal\ atom}$ (Figure 1c,d, Supporting Figures 1–3). The doping of Zn^{2+} ion increases the overall magnetic moments of typical ferrite-based nanomaterials,[23] which gives increased magnetic gradient force per particle. The electromagnet (EM) probe is custom-built and comprises a NiFe permalloy probe tip (tip diameter: *ca.* 10 μm) housed inside a water cooling system.[24] This EM probe is controlled with a function generator and an amplifier such that it can generate oscillating magnetic fields up to 10 000 Hz. The measured magnetic field gradient is *ca.* 1000 $T \cdot m^{-1}$ at a 10 μm distance from the tip (Supporting Figure 4), leading to *ca.* 0.1 pN of force for a single c-MNP at the same distance. In addition, the colloidal stability and chemical functionality are enhanced by coating the c-MNPs with silica and polyethylene glycol (PEG). Sequential treatments with tetraethylorthosilicate (TEOS) and aminopropyltrimethoxysilane (APTMS) introduce a silica coating of 3.8 nm thickness, onto which carboxylated-PEGs are

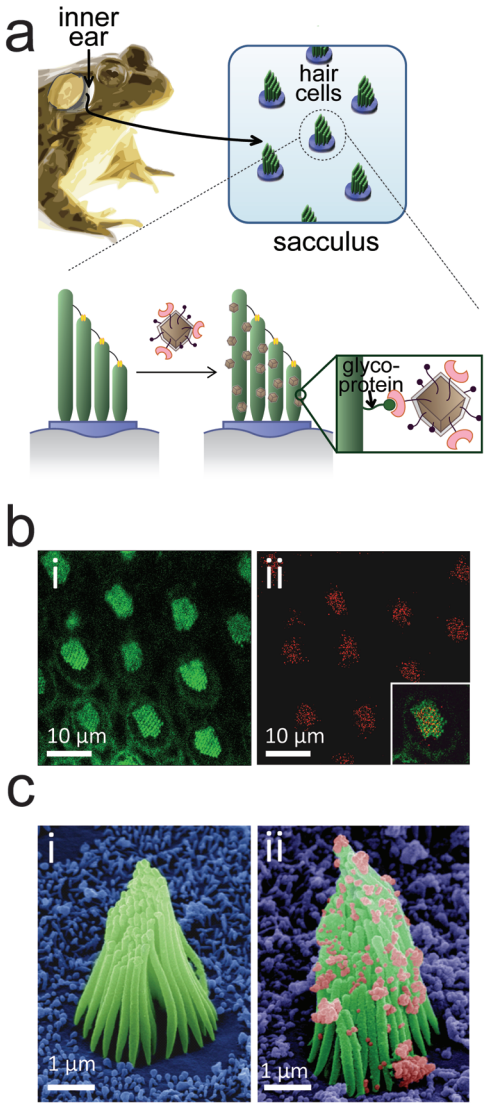

Figure 2. Conjugation of c-MNPs to hair cells of the amphibian inner ear. (a) Hair cells prepared from the sacculus of the bullfrog (*Rana catesbeiana*) and treatment with conA/c-MNP conjugates. The conA/c-MNP conjugates are bound to the stereocilia of a hair bundle through the glycoprotein–conA interaction. (b) Confocal microscope images of hair bundles treated with conA/c-MNPs. (i) Actin, constituting the core of the stereocilia, was stained with Alexa-488-phalloidin, and (ii) conA/c-MNPs were stained with rhodamine. Fluorescence signals of stereocilia and c-MNPs colocalize. Inset: Merged image of (i) and (ii) for a single hair bundle. (c) Scanning electron microscopy (SEM) images of a single hair bundle (i) before and (ii) after conA/c-MNP treatment. SEM images are false-colored for clarity, showing the hair bundle in green, the cuticular plate in blue, and the c-MNPs in pink.

chemically conjugated (Figure 1b, Supporting Figure 1). The dynamic light scattering measurements reveal a hydrodynamic size of *ca.* 65 nm after these modifications (Supporting Figure 3). The modified c-MNPs are stable colloids in aqueous media. The surface passivation of c-MNP with silica and PEG is effective to prevent potential aggregation despite its weak ferromagnetic nature (Supporting Figure 2).[25] Also, a fluorescent rhodamine dye is embedded inside the silica layer to provide optical visibility under fluorescence microscopy.

Inner Ear Hair Cells: A Fast Mechanotransduction System. In our study, sensory epithelia, containing hair cells embedded in the supporting tissue, are obtained from the sacculus of the North American bullfrog (*Rana catesbeiana*); the epithelia are carefully dissected and maintained in a chemical environment that preserves the delicate mechanotransduction system.[5] The c-MNP is conjugated to concanavalin A (conA), a type of lectin that binds to glycoproteins abundant on the hair bundle surface; the conjugation is achieved by using 1-ethyl-3-(3-(dimethylamino)propyl) carbodiimide (EDC) and *N*-hydroxysulfosuccinimide (sulfo-NHS) as cross-linkers (Figures 1b, 2a). Figure 2b shows hair bundles stained in green Alexa-488-phalloidin and conA/c-MNP conjugates stained in red with rhodamine embedded in the silica coating layer. Confocal images indicate that the fluorescence of c-MNPs is largely colocalized with that of the hair bundles, indicating preferential binding of the conA/c-MNPs to the bundles. Electron microscope images also confirm the binding of conA/c-MNPs to the hair bundles (Figure 2c; see also Supporting Figure 5).

The dissected sacculus, conjugated with conA/c-MNPs, is placed in an upright optical microscope and imaged under bright-field illumination, with a top-down view of the hair bundles. The EM probe tip is brought into the vicinity of a selected hair cell (to within 10 μm distance) (Figure 3a). Electric current applied to the magnetic probe generates a magnetic force on the MNPs (Supporting Figure 4), which can deflect the hair bundle to which they are attached. The collective force exerted by the c-MNPs on the hair bundle (typical stiffnes of $\sim$1 mN$\cdot$m^{-1}) deflects it by 10–100 nm (Figure 3b,c). The induced mechanical displacements of the hair bundle are recorded with a high-speed CMOS camera (FASTCAM SA1.1, Photron Inc.) at 100–100 000 fps. Movements of the bundle are tracked with software developed in MATLAB.[26]

Magnetic Stimulation and Entrainment. The response of a representative hair bundle is shown in Figure 3c, with black and red lines representing the bundle position and the current sent to the magnetic probe, respectively. When the probe is in the OFF state (–10 mA, which leads to demagnetization of the probe), the hair bundle oscillates freely with an average amplitude of *ca.* 30 nm, which is referred to as spontaneous oscillation.[27] In contrast, when the magnetic probe is in the ON state (100 mA), the bundle is deflected toward the probe by $\sim$50 nm (Figure 3c(i)), ceasing the spontaneous oscillation and maintaining the quiescent state during the ON phase of the stimulus. Tracking of the more remote bundles in the same field of view shows that their motion is not affected by the magnetic stimulation, as the magnetic force falls off rapidly with distance from the probe (Supporting Figure 4). If the magnetic field is pulsed (*e.g.*, at 5 Hz), the bundle

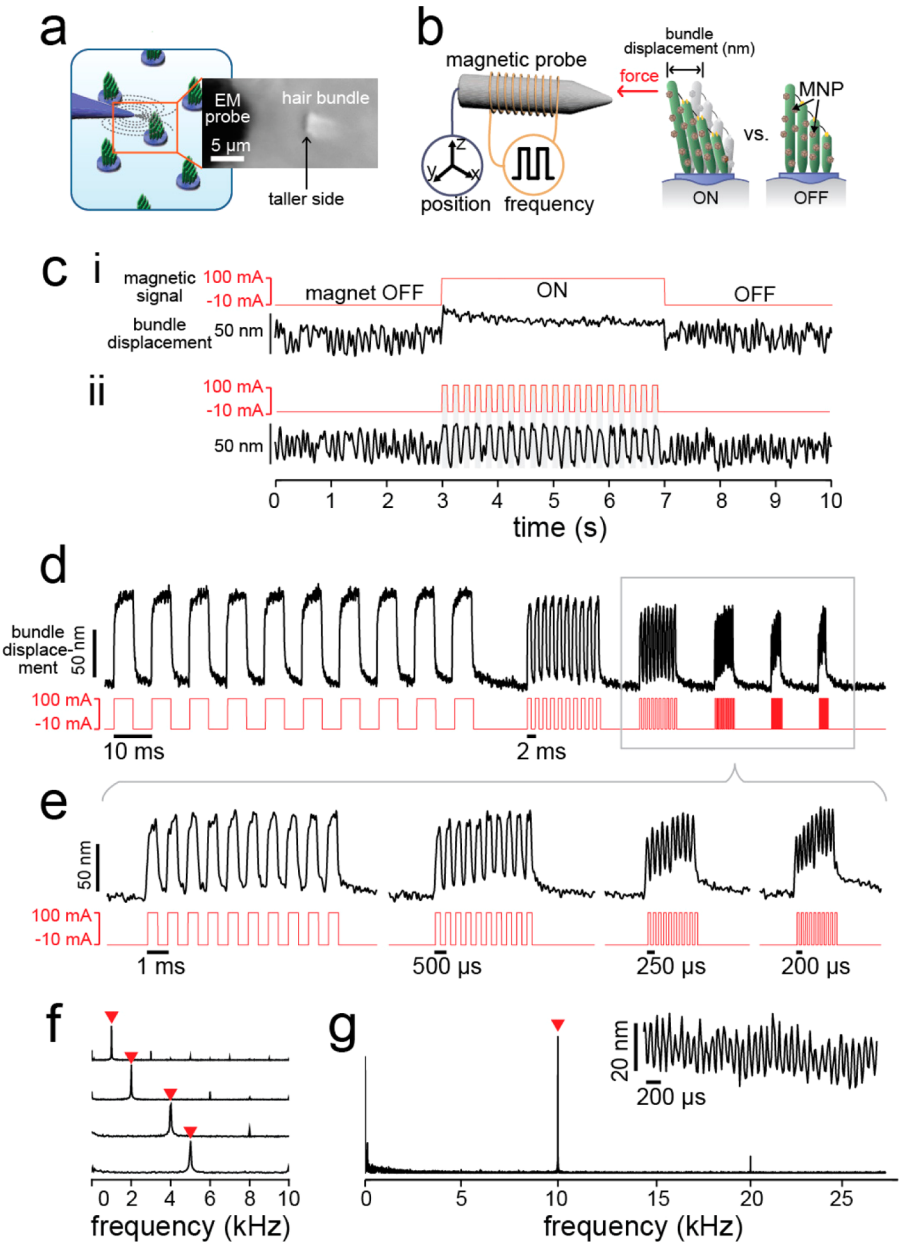

Figure 3. Entrainment of hair bundle oscillation with a magnetic switch. (a) Schematic drawing of a magnetic probe activating a single hair bundle and a bright-field microscope image in top-down view. (b) Schematic diagram of the EM probe stimulating a single hair bundle with c-MNPs attached. (c) Motion of a single hair bundle deflected by the EM probe. Black line: tracked bundle displacement, red line: current applied to the EM probe. Spontaneous oscillation of the bundle is modulated by the application of (i) static and (ii) 5 Hz square wave current. (d) Stimulation frequency variation: pulse frequencies of 100, 500, 1000, 2000, 4000, and 5000 Hz are applied to entrain the bundle motility. (e) Enlarged view of (d). (f) Fourier transform (FT) spectra of entrained bundle oscillation shown in (e). (g) FT spectrum of bundle motions, entrained at 10 000 Hz. The inset shows the tracked bundle displacement.

movement is entrained at the frequency of the stimulus (Figure 3c(ii)). All these processes are reversible, with the bundle recovering its spontaneous oscillation when the magnetic probe is switched to the OFF state.

To assess the temporal control achievable with this system, we examined the entrainment of hair bundles at higher frequencies. Figure 3d shows the results obtained from a hair bundle conjugated with c-MNPs and stimulated at 100, 500, 1000, 2000, 4000, 5000, and 10 000 Hz. Bundle deflection was entrained by the stimulating magnetic fields and remained phase-locked over the frequency range tested; black and red lines represent the bundle displacement and the magnetic pulses sent to the EM probe, respectively (Figure 3d). Enlarged plots show that clear entrainment persists even up to 10 000 Hz (Figure 3e,g), as is also demonstrated in the Fourier spectrum (Figure 3f,g). The amplitude of the entrained bundle oscillation decreases at higher frequencies because the bundle is not fully relaxed to its original position between

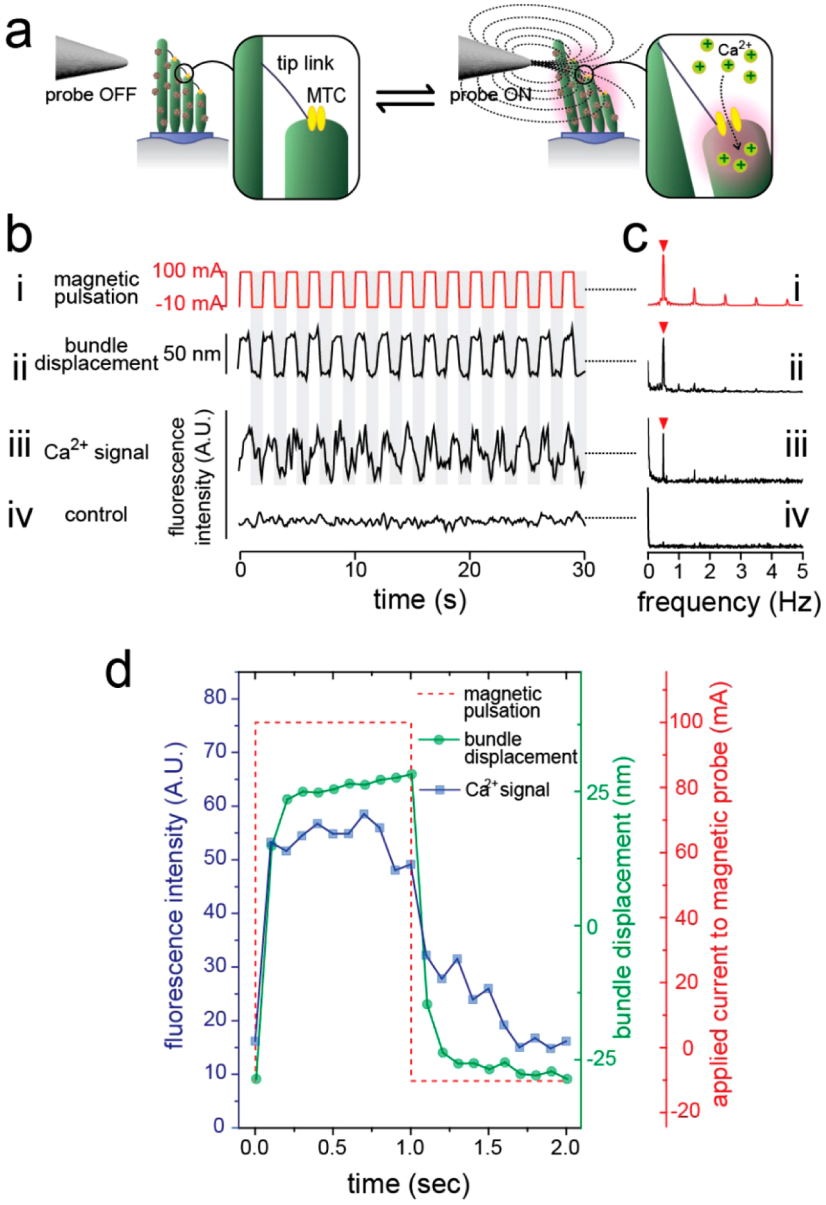

Figure 4. Magnetism-controlled gating of the mechanotransduction process. (a) Schematic drawing of the magnetically gated manipulation, leading to the opening and closing of ion channels. Mechanical tension in the tip links, induced by hair bundle deflection, opens the ion channels, allowing an influx of Ca^{2+}. (b) Traces of (i) pulsed magnetic stimulation, (ii) the resulting hair bundle displacement, and (iii) the Fluo-4 (a Ca^{2+}-sensitive dye) fluorescence signal in the bundle. The control experiment, performed on a hair bundle in which the tip links were severed by BAPTA, thus abolishing transduction, is shown in (iv). (c) Corresponding FT spectra of (b), which indicate that the fluorescence signals are observed at the frequency of the magnetic pulse train. (d) Ca^{2+} fluorescence and bundle displacement for a single magnetic pulse, averaged over 50 presentations.

consecutive magnetic pulses. Considering the hearing range of animals (*e.g.*, human 0.02−20 kHz, frog 0.1−1.4 kHz),[28] the high frequencies achieved with our magnetic probes can be used to study the auditory mechanotransduction system across a broad range of species. Considering that the temporal resolution of the state-of-the-art magnetic system is still in the range of a few seconds scale,[14,20] our sub-millisecond temporal window can be remarkably advantageous for the study of a wide range of mechanosensitive biological systems.

Activation of the Mechanotransduction Channels. We next explored whether magnetic deflection of the hair bundle can lead to a temporally controlled gating of the mechanosensitive ion channels. When the bundle is deflected toward the taller side of the bundle, the mechanical tension conveyed to the tip link leads to the opening of transduction channels, allowing an influx of potassium and calcium ions (Figure 4a).[29] To investigate the gating of ion channels during the magnetic stimulation, relative levels of intracellular Ca^{2+} concentration are monitored with fluorescence

microscopy. The hair cell preparation is incubated with Fluo4-AM dye (6 μM) for 30 min prior to the conA/c-MNP treatment. The hair cell is imaged in a sideways configuration under fluorescence microscopy, and the fluorescence signal from the bundle region is recorded with an EMCCD camera (Andor iXon+) (Supporting Figure 6). Figure 4b shows (i) the trace of a square-wave train of magnetic pulses, (ii) the resulting bundle deflection, and (iii) the measured Ca^{2+} fluorescence intensity of the bundle. The change in the bundle fluorescence coincides with the magnetic stimulus and the induced bundle deflection (Figure 4b(i−iii)), with deflections in the positive direction corresponding to the preferential opening of the channels and hence an influx of the Ca^{2+} ions. The same peaks at 0.5 Hz are observed in the Fourier transforms of the two traces (Figure 4c). In a control experiment, tip links were damaged by treatment with *N*,*N*-[1,2-ethanediylbis(oxy-2,1-phenylene)]bis-[*N*-[2-[(acetyloxy)methoxy]-2-oxoethyl]] bis-[(acetyloxy)methyl] ester (BAPTA; 5 mM);[30] under identical stimulus, a change in the fluorescence signal of the bundle was not observed (Figure 4b,c(iv)). The results, averaged over 50 cycles, are shown in Figure 4d, with red, green, and blue lines representing the averaged magnetic pulse, bundle displacement, and Ca^{2+} signal, respectively (Figure 4d). The intensity of the Ca^{2+} signal rises with a positive bundle displacement; a delay occurs in the decrease of the Ca^{2+} signal during the OFF state of the magnetic stimulus. This time delay of the Ca^{2+} signal may reflect the buffering and extrusion dynamics of Ca^{2+} and its dissociation from the dye.[30]

The fast and reversible magnetism-gated switch developed here provides several important advantages over other methods currently available for auditory hair bundle stimulation. Glass pipettes or piezoelectric probes have been used for the same purpose;[5,6] however, viscoelastic loading of the bundle by an attached probe has been shown to affect the intrinsic spontaneous oscillation and the mechanical response of the cell.[7] The long and flexible glass probe also imposes a filter on the stimulus sent to the bundle, rendering it difficult to obtain frequencies of stimulation higher than 1 kHz.[31] The magnetic switch, on the contrary, can apply forces at frequencies up to 10 kHz without significant time lags. Moreover, the EM probe remains stationary during the stimulation, thus avoiding any hydrodynamic artifacts that can affect the bundle motion when it is stimulated by a probe vibrating in a fluid environment or by a water jet stream.[5,32]

CONCLUSION

The magnetic switch, which uses cube-shaped magnetic nanoparticles, is exceptionally well suited for accomplishing fast and reversible mechanical stimulation that is spatiotemporally controlled at a single cell level. It is applicable not only to the auditory system but to a broad range of sensory systems with mechanosensitive channels. In addition, the use of a magnetic field, to which biological tissue is transparent, can be beneficial for remote and non-invasive stimulation of a wide range of biological targets.

METHODS/EXPERIMENTAL SECTION

Synthesis of Cube-Shaped Magnetic Nanoparticles. All chemicals were purchased from Sigma-Aldrich unless specified otherwise. Iron(III) acetylacetonate, zinc chloride, and cobalt(II) acetylacetonate were used as received. Oleic acid and oleylamine were purified by distillation under an argon atmosphere. The 45 nm sized c-MNPs were synthesized by using the protocol previously developed in our group, which is described in Noh *et al.*[25] Briefly, iron(III) acetylacetonate (0.8 mmol) and zinc(II) acetylacetonate (1.2 mmol) were placed in a 25 mL three-neck round-bottom flask in the presence of oleic acid (3.78 mmol) and benzyl ether (52.61 mmol). The mixture was heated for 30 min at 290 °C under an argon atmosphere and cooled to room temperature. Under ambient conditions, ethanol was added to the mixture, resulting in a black precipitate; it was then centrifuged, isolated, and dispersed in toluene. The transmission electron microscope (TEM) image of as-synthesized c-MNP is shown in Supporting Figure 1b; the size of the particle is *ca.* 45 nm along one edge. Investigation of the nanoparticle, using the energy-dispersive X-ray spectroscopy (EDS) add-on in TEM and the inductively coupled plasma−atomic emission spectra (ICP-AES), reveals that the stoichiometry of the nanoparticle is $Zn_{0.4}Fe_{2.6}O_4$. Also, the X-ray diffraction pattern of the c-MNP indicates the spinel crystal structure.

The surface of c-MNP was then modified with silica to harness its hydrophilic properties. To coat the particle with a SiO_2 shell that is 3.8 nm thick, 780 μL of Igepal CO-520 and 1.2 mg of c-MNPs were dispersed in 12 mL of cyclohexane. Then, 105 μL of ammonium hydroxide (30%) was added while vortexing, and the mixture was sonicated for 1 min, followed by the addition of 30 μL of tetraethylorthosilicate (TEOS). After shaking at 120 rpm for 48 h, 6 μL of (3-aminopropyl)-trimethoxysilane (APTMS) was added and incubated for additional 24 h at room temperature. When the reaction was finished, 3 mL of methanol was added to precipitate out the cube $Zn_{0.4}Fe_{2.6}O_4$@SiO_2 nanoparticles by centrifugation (500 rpm, 1 min). An image of the resulting nanoparticles is shown in Supporting Figure 1c, which shows a 3.8 nm coating of silica on the c-MNP.

In the next step, polyethylene glycol was conjugated on the surface of the nanoparticle to enhance colloidal stability and to serve as an antibiofouling agent. Prior to PEG conjugation, the surface of the nanoparticle was activated with 2 mM succinic anhydride (SA) in DMSO in an overnight reaction. During this reaction, primary amine groups on the nanoparticle surface were substituted with carboxylate groups. After washing excess amounts of SA by centrifugation at least three times, the nanoparticles were dissolved into 1 mL of phosphate buffer solution (10 mM, pH 7.4). Then, carboxy-PEGn-amine (3 mg, MW = 3400, Nanocs Inc.), 1-ethyl-3-(3-(dimethylamino)propyl)carbodiimide (5 mM, Pierce Biotech Inc.), and *N*-hydroxysulfosuccinimide (2 mM, Pierce Biotech Inc.) were added to the nanoparticle solution and reacted for 2 h at room temperature. The final products were collected from the solution by centrifugation.

Magnetism Measurement of c-MNPs. Magnetic properties of c-MNPs were measured with a superconducting quantum

interference device (SQUID, Quantum Design MPMS7), to obtain the magnetization (*M*) *vs* magnetic field (*H*) curve (Figure 1d, Supporting Figure 2). The measurement was performed at room temperature (25 °C). The measured sample was further analyzed with ICP-AES to find the exact mass of the metallic component in the nanoparticle and to calibrate the magnetization value.

Assessment of Colloidal Stability of c-MNPs. The hydrodynamic size of c-MNPs was measured with a dynamic light scattering (DLS) instrument (Zetasizer, Malvern Instrument). The c-MNPs were dissolved in an aqueous solution at a concentration of 0.5 mg/mL, and the distribution of their hydrodynamic sizes is shown in Supporting Figure 3. The highest peak appears at 65 nm, and its distribution ranges from ~20 to 120 nm, which indicates that 20−40% of the nanoparticles are in the state of homogeneously dispersed single nanoparticles. The nanoparticles form sedimentation due to gravity, but can be dispersed back to the initial state by pipetting and sonication.

Fabrication of the Electromagnetic Probe. The EM probe used in these experiments is manufactured following the general procedures described by Matthews *et al*., with slight modifications.[24] Briefly, the electromagnet consists of a copper wire coil, a plastic capillary tube, a water jacket, and a permalloy magnetic probe tip. The resistance of the coil was 70 Ω. The coil was placed within a water circulation jacket to prevent overheating of the electromagnet. A permalloy 80 (ESPI metals) rod (1 mm diameter; 30 mm length) was used as the electromagnet core material.

Calibration of the Magnetic Field Gradient Produced by the Magnetic Probe Tip. The electromagnet probe tip was mounted under an upright optical microscope (Olympus B51X) with a water-immersion objective lens (60×, 0.9 NA). The magnetic field gradient $\vec{\nabla}B$ generated by the probe tip was calibrated by tracking the velocity of magnetic beads (1 μm diameter, 50 μg·mL^{-1}, Sera-Mag, Fisher Scientific) immersed in a solution of 80% glycerol. The magnetic force is counterbalanced by the viscous force given by the Stokes law: $\mu\vec{\nabla}B = 3\pi\eta d\vec{v}$, where $\mu = 6.5 \times 10^{-14}$ A·m^2 is the magnetic moment of an individual magnetic bead, $\eta = 6.14 \times 10^{-2}$ Pa·s is the 80% glycerol solution viscosity, $d = 1.1$ μm is the mean bead diameter, and $\vec{v}$ is the bead velocity. The trajectories of around 200 magnetic beads were recorded either at 33 fps on a 100 × 100 μm^2 field of view or at 114 fps on a 30 × 30 μm^2 field of view using an Andor iXon+ EMCCD camera. The trajectories were analyzed with the particle-tracking algorithm developed by the MOSAIC Group[33] (Supporting Figure 4a). The 2D field gradient map was then constructed using software developed with Mathematica 9 (Wolfram) (Supporting Figure 4b).

Force Calculation on the Nanoparticle. To calculate the force exerted on the c-MNP by the gradient of the magnetic field, we use the measured value of the one-dimensional d*B*/d*x*, the magnetization of the particle (*m*), and the size of the particle. The mass of a single c-MNP is calculated to be 6.6×10^{-16} g, using the known volume (cube of 50 nm edge) and the mean density of ferrite materials (5300 kg·m^{-3}). Assuming that nanoparticles are magnetically saturated in the applied field gradient, the magnetic moment of a single c-MNP is calculated to be *ca*. 1×10^{-13} emu (= 1×10^{-16} A·m^2), using the saturation magnetization of 162 emu·g^{-1} and the mass of a single c-MNP. The force exerted is a product of the field gradient and the magnetic moment; therefore, a c-MNP experiences *ca*. 0.1 pN of force under 1000 T·m^{-1}.

Hair Cell Preparation. Prior to performing the experiments, all animal-handling protocols were approved by the UCLA Chancellor's Animal Research Committee (Protocol Number ARC 2006-043-13C) in accordance with federal and state guidelines. Experiments were performed on *in vitro* preparations of the sacculus,[34] excised from the inner ear of the North American bullfrog (*Rana catesbeiana*). The preparations were mounted in a two-compartment chamber, with hair cells exposed to artificial perilymph and endolymph on the basal and apical sides, respectively. The solutions were made to mimic the ionic conditions in the sacculus; for perilymph, it contained (in mM) 110 Na^+, 2 K^+, 1.5 Ca^{2+}, 113 Cl^-, 3 D-glucose, 1 sodium pyruvate, 1 creatine, 5 HEPES; and for endolymph: 2 Na^+, 118 K^+, 0.25 Ca^{2+}, 118 Cl^-, 3 D-glucose, 5 HEPES. Both solutions were oxygenated for ~10 min prior to use. The overlying otolithic membrane was removed from the epithelium with an eyelash tool, following a 7−8 min enzymatic dissociation with 15 μg·mL^{-1} collagenase IV (Sigma-Aldrich). Active spontaneous oscillation was observed in hair bundles after decoupling from the membrane and could be maintained for several hours postdissection. For the high-frequency entrainment experiments, the spontaneous oscillation was artificially suppressed for the clear entrainment visibility, by introducing perilymph on top of the preparation instead of endolymph.

c-MNP Conjugation to the Hair Cell Bundle. After dissolving c-MNPs in 0.5 mL of 10 mM phosphate buffer solution (pH 7.4) to obtain 0.1 mg·mL^{-1} of concentration, EDC (0.2 mg) and sulfo-NHS (0.4 mg) were dissolved in the same solution to activate the surface of the nanoparticles for 15 min. After the surface of nanoparticles was activated, 0.6 mg of concanavalin A type VI was dissolved in the solution and reacted for 40 min with gentle shaking. When the reaction was finished, the c-MNP/conA conjugates were isolated by centrifugation at 2500 rcf, twice for 4 min. The resulting nanoparticle conA conjugates were dissolved in 100 μL of artificial perilymph, leading to a concentration of nanoparticles of roughly 0.1 mg·mL^{-1}. One drop (~50 μL) of the nanoparticle conjugates was added to the solution on top of the hair bundle preparation, described in the previous section, for 30 min. After the binding of c-MNPs to the hair bundles *via* conA and glycoprotein interaction at the hair cell surface, the remaining excess amounts of c-MNPs were gently washed with perilymph solution, two to three times. Supporting Figure 5 is the TEM image of c-MNP attached to a hair bundle.

Detection of Hair Bundle Motility. Preparations were imaged in an upright optical microscope (Olympus B51X) with a water immersion objective (20×, 0.95 NA) and illuminated with an X-Cite 120 W Mercury arc lamp. Images were further magnified to ~400× and projected onto a high-speed complementary metal oxide semiconductor (CMOS) camera (Photron FASTCAM SA1.1) at 100−100 000 kHz. The motion of the hair bundles was tracked with software written in MATLAB (The MathWorks).[35] A horizontal line scan was taken through the image in each frame, and a Gaussian distribution was fit to the intensity profile of the bundle to extract the center position. To improve the signal-to-noise ratio, vertically adjacent pixel rows were tracked and averaged. Time-dependent traces of the movement were then obtained by plotting the extracted center position of the bundle for each frame of the record. The noise levels in these recordings were ~3−5 nm.

Magnetic Stimulation of a Hair Bundle. For the entrainment of hair bundle oscillation, the magnetic probe tip was mounted on a motorized micromanipulator (Siskiyou Inc.). The magnetic probe tip was positioned close to the target hair bundle, conjugated with magnetic nanoparticles. The distance from the probe tip to the bundle was adjusted to be within 10 μm, with the tallest side of the bundle (the kinocilium side) facing toward the magnetic probe tip. The electric potential applied to the magnetic probe tip was tuned to compensate for the inductance of the coil and obtain a square wave current from −10 to 100 mA in the coil. A current of 100 mA was applied to magnetize the probe tip, and −10 mA was applied to demagnetize the probe tip. The potential was generated by an analog output module from National Instrument (NI 9263), connected to an amplifier (PZ-150M, Burleigh), and the current applied to the magnetic probe was monitored by an analog input module from National Instrument (NI 9215). The waveform for the applied potential was generated using LabVIEW software (National Instrument), to produce step functions with frequencies from 100 to 10 000 Hz. CMOS camera recording was synchronized with the stimulus. Deflection imposed on the bundles was measured from the video recordings by subtracting the bundle position under deflection from the original position.

Calcium Imaging of a Hair Bundle. For the calcium imaging performed in conjunction with magnetic stimulation, the hair bundles were incubated with Fluo-4 AM dye (Life Technology Co.), following protocols developed by Lumpkin *et al*. with slight modifications. The saccular preparation was placed in a two-compartment chamber, with perilymph on top instead of

endolymph. The concentration of Fluo-4 AM in perilymph was 6 μM. The preparation was incubated with nanoparticles at the same time, at a concentration of 0.1 mg/mL. After 30 min, the preparation was washed three times with perilymph. For the control experiment with broken tip links, the preparation was treated with *N,N'*-[1,2-ethanediylbis(oxy-2,1-phenylene)]bis-[*N*-[2-[(acetyloxy)methoxy]-2-oxoethyl]] bis[(acetyloxy)methyl] ester (BAPTA-AM, Life Technology Co.; 5 mM) for 15 min. To observe the hair bundle in a side view, the preparation was gently folded in half in the perilymph solution and placed under the optical microscope. Magnetic stimulation of the hair bundle was done as described previously. The advantage of the side view for calcium imaging is that the weak fluorescence signal from the hair bundle can be more easily differentiated from the background signal from the cell body. An LED light source (M505L2-C1, Cyan, Thorlab) was used to illuminate the bundle. The frequency of the applied current was adjusted to 0.5 Hz. Calcium signal was recorded with an electron multiplying CCD (EMCCD) camera (iXon+, Andor Co.), at a fixed gain. Camera recording and stimulation current were synchronized with a signal sent from the function generator (AFG 3000, Tektronix). The intensity of the calcium signal in the bundle region was analyzed with ImageJ (NIH) and Matlab (Mathworks). A region of interest around the hair bundle was selected for the recording, and the mean signal intensity was measured for each frame. Supporting Figure 6 shows the representative calcium fluorescence image.

Conflict of Interest: The authors declare no competing financial interest.

Acknowledgment. This research was supported by the U.S. Air Force Office of Scientific Research (grant number FA9550-12-1-0407 for D.B. and J.C.), National Creative Research Initiative (2010-0018286 for J.C.), and the Korea Healthcare Technology R&D Project, Ministry for Health & Welfare Affairs, Republic of Korea (HI08C2149 for J.C.). Confocal laser scanning microscopy was performed at the CNSI ALMS facility at UCLA (NIH-NCRR grant CJX1-443835-WS-29646; NSF grant CHE-0722519). We thank Prof. Katsushi Arisaka, Prof. Giovanni Zocchi, Dr. Matthew Schibler, and Mr. Peter Yu for helpful discussions.

Supporting Information Available: TEM images and magnetic properties of the nanoparticles. Magnetic force measurements. TEM image of nanoparticles binding to the hair cell. Calcium imaging results. This material is available free of charge *via* the Internet at http://pubs.acs.org.

REFERENCES AND NOTES

1. Gillespie, P. G.; Walker, R. G. Molecular Basis of Mechanosensory Transduction. *Nature* **2011**, *413*, 194–202.
2. Coste, B.; Mathur, J.; Schmidt, M.; Earley, T. J.; Ranade, S.; Petrus, M. J.; Dubin, A. E.; Patapoutian, A. Piezo1 and Piezo2 Are Essential Components of Distinct Mechanically Activated Cation Channels. *Science* **2010**, *330*, 55–60.
3. Wang, N.; Tytell, J. D.; Ingber, D. E. Mechanotransduction at a Distance: Mechanically Coupling the Extracellular Matrix with the Nucleus. *Nat. Rev. Mol. Cell Biol.* **2009**, *10*, 75–82.
4. DuFort, C. C.; Paszek, M. J.; Weaver, V. M. Balancing Forces: Architectural Control of Mechanotransduction. *Nat. Rev. Mol. Cell Biol.* **2011**, *12*, 308–319.
5. Roongthumskul, Y.; Fredrickson-Hemsing, L.; Kao, A.; Bozovic, D. Multiple-Timescale Dynamics Underlying Spontaneous Oscillations of Saccular Hair Bundles. *Biophys. J.* **2011**, *101*, 603–610.
6. Doll, J. C.; Peng, A. W.; Ricci, A. J.; Pruitt, B. L. Faster Than the Speed of Hearing: Nanomechanical Force Probes Enable the Electromechanical Observation of Cochlear Hair Cells. *Nano Lett.* **2012**, *12*, 6107–6111.
7. Strimbu, C. E.; Fredrickson-Hemsing, L.; Bozovic, D. Coupling and Elastic Loading Affect the Active Response by the Inner Ear Hair Cell Bundles. *PLoS One* **2012**, *7*, e33862.
8. Pratt, K. W.; Johnson, D. C. Vibrating Wire Electrodes - I. Literature Review, Design and Evaluation. *Electrochim. Acta* **1982**, *27*, 1013–1021.
9. Boyden, E. S.; Zhang, F.; Bamberg, E.; Nagel, G.; Deisseroth, K. Millisecond-Timescale, Genetically Targeted Optical Control of Neural Activity. *Nat. Neurosci.* **2005**, *8*, 1263–1268.
10. Lohmann, K. J. Magnetic-Field Perception. *Nature* **2010**, *464*, 1140–1142.
11. Walker, M. M.; Diebel, C. E.; Haugh, C. V.; Pankhurst, P. M.; Montgomery, J. C.; Green, C. R. Structure and Function of the Vertebrate Magnetic Sense. *Nature* **1997**, *390*, 371–376.
12. Pankhurst, Q. A.; Connolly, J.; Jones, S. K.; Dobson, J. Applications of Magnetic Nanoparticles in Biomedicine. *J. Phys. D: Appl. Phys.* **2003**, *36*, R167.
13. Etoc, F.; Lisse, D.; Bellaiche, Y.; Piehler, J.; Coppey, M.; Dahan, M. Subcellular Control of Rac-GTPase Signalling by Magnetogenetic Manipulation Inside Living Cells. *Nat. Nanotechnol.* **2013**, *8*, 193–198.
14. Hoffmann, C.; Mazari, E.; Lallet, S.; Le Borgne, R.; Marchi, V.; Gosse, C.; Gueroui, Z. Spatiotemporal Control of Microtubule Nucleation and Assembly Using Magnetic Nanoparticles. *Nat. Nanotechnol.* **2013**, *8*, 199–205.
15. Cho, M. H.; Lee, E. J.; Son, M.; Lee, J.-H.; Yoo, D.; Kim, J.-w.; Park, S. W.; Shin, J. S.; Cheon, J. A Magnetic Switch for the Control of Cell Death Signalling in *in Vitro* and *in Vivo* Systems. *Nat. Mater.* **2012**, *11*, 1038–1043.
16. Dobson, J. Remote Control of Cellular Behaviour with Magnetic Nanoparticles. *Nat. Nanotechnol.* **2008**, *3*, 139–143.
17. Mannix, R. J.; Kumar, S.; Cassiola, F.; Montoya-Zavala, M.; Feinstein, E.; Prentiss, M.; Ingber, D. E. Nanomagnetic Actuation of Receptor-Mediated Signal Transduction. *Nat. Nanotechnol.* **2008**, *3*, 36–40.
18. Huang, H.; Delikanli, S.; Zeng, H.; Ferkey, D. M.; Pralle, A. Remote Control of Ion Channels and Neurons through Magnetic-Field Heating of Nanoparticles. *Nat. Nanotechnol.* **2010**, *5*, 602–606.
19. Stanley, S. A.; Gagner, J. E.; Damanpour, S.; Yoshida, M.; Dordick, J. S.; Friedman, J. M. Radio-Wave Heating of Iron Oxide Nanoparticles Can Regulate Plasma Glucose in Mice. *Science* **2012**, *336*, 604–608.
20. Hughes, S.; McBain, S.; Dobson, J.; El Haj, A. J. Selective Activation of Mechanosensitive Ion Channels Using Magnetic Particles. *J. R. Soc. Interface* **2008**, *5*, 855–863.
21. Hudspeth, A. J. Making an Effort to Listen: Mechanical Amplification in the Ear. *Neuron* **2008**, *59*, 530–545.
22. Gillespie, P. G.; Müller, U. Mechanotransduction by Hair Cells: Models, Molecules, and Mechanisms. *Cell* **2009**, *139*, 33–44.
23. Jang, J.-t.; Nah, H.; Lee, J.-H.; Moon, S. H.; Kim, M. G.; Cheon, J. Critical Enhancements of MRI Contrast and Hyperthermic Effects by Dopant-Controlled Magnetic Nanoparticles. *Angew. Chem., Int. Ed.* **2009**, *48*, 1234–1238.
24. Matthews, B. D.; LaVan, D. A.; Overby, D. R.; Karavitis, J.; Ingber, D. E. Electromagnetic Needles with Submicron Pole Tip Radii for Nanomanipulation of Biomolecules and Living Cells. *Appl. Phys. Lett.* **2004**, *85*, 2968–2970.
25. Noh, S.-h.; Na, W.; Jang, J.-t.; Lee, J.-H.; Lee, E. J.; Moon, S. H.; Lim, Y.; Shin, J.-S.; Cheon, J. Nanoscale Magnetism Control *via* Surface and Exchange Anisotropy for Optimized Ferrimagnetic Hysteresis. *Nano Lett.* **2012**, *12*, 3716–3721.
26. Ramunno-Johnson, D.; Strimbu, C. E.; Frederickson, L.; Arisaka, K.; Bozovic, D. Distribution of Frequencies of Spontaneous Oscillations in Hair Cells of the Bullfrog Sacculus. *Biophys. J.* **2009**, *96*, 1159–1168.
27. Martin, P.; Bozovic, D.; Choe, Y.; Hudspeth, A. J. Spontaneous Oscillation by Hair Bundles of the Bullfrog's Sacculus. *J. Neurosci.* **2003**, *23*, 4533–4548.
28. Peng, A. W.; Ricci, A. J. Somatic Motility and Hair Bundle Mechanics, Are Both Necessary for Cochlear Amplification? *Hearing Res.* **2011**, *273*, 109–122.
29. Kachar, B.; Parakkal, M.; Kurc, M.; Zhao, Y.-d.; Gillespie, P. G. High-Resolution Structure of Hair-Cell Tip Links. *Proc. Natl. Acad. Sci. U.S.A.* **2000**, *97*, 13336–13341.
30. Eatock, R. A. Adaptation in Hair Cells. *Annu. Rev. Neurosci.* **2000**, *23*, 285–314.

31. Ohmori, H. Mechanical Stimulation and Fura-2 Fluorescence in the Hair Bundle of Dissociated Hair Cells of the Chick. *J. Physiol.* **1988**, *399*, 115–137.
32. Beurg, M.; Fettiplace, R.; Nam, J.-H.; Ricci, A. J. Localization of Inner Hair Cell Mechanotransducer Channels Using High-Speed Calcium Imaging. *Nat. Neurosci.* **2009**, *12*, 553–558.
33. Sbalzarini, I.; Koumoutsakos, P. Feature Point Tracking and Trajectory Analysis for Video Imaging in Cell Biology. *J. Struct. Biol.* **2005**, *151*, 182–195.
34. Narins, P. M.; Lewis, E. R. The Vertebrate Ear As an Exquisite Seismic Sensor. *J. Acous. Soc. Am.* **1984**, *76*, 1384–1387.
35. Kao, A.; Meenderink, S. W. F.; Bozovic, D. Mechanical Overstimulation of Hair Bundles: Suppression and Recovery of Active Motility. *PLoS One* **2013**, *8*, e58143.